

# Fast Approximate Clearance Evaluation for Kinematically Constrained Articulated Suspension Systems

Kyohei Otsu<sup>1</sup>, Guillaume Matheron<sup>2</sup>, Sourish Ghosh<sup>3</sup>, Olivier Toupet<sup>1</sup>, and Masahiro Ono<sup>1</sup>

**Abstract**—In this paper, we present a light-weight collision detection algorithm for motion planning of planetary rovers with articulated suspension systems. Extraterrestrial path planning is challenging due to the combination of terrain roughness and severe limitation in computational resources. Path planning on cluttered and/or uneven terrains requires repeated collision detection on all the candidate paths at a small interval. Solving the exact collision detection problem for articulated suspension systems requires simulating the vehicle settling on the terrain, which involves an inverse-kinematics problem with iterative nonlinear optimization under geometric constraints. However, such expensive computation is intractable for slow spacecraft computers, such as the RAD750 that is used by the Curiosity Mars rover and upcoming Mars 2020 rover. We propose the Approximate Clearance Evaluation (ACE) algorithm, which obtains conservative bounds on vehicle clearance, attitude, and suspension angles *without* iterative computation. It obtains those bounds by estimating the lowest and highest heights that each wheel may reach given the underlying terrain, and calculating the worst-case vehicle configuration associated with those extreme wheel heights. The bounds are guaranteed to be conservative, hence ensuring vehicle safety during autonomous navigation. ACE is planned to be used as part of the new onboard path planner of the Mars 2020 rover. This paper describes the algorithm in detail and validates our claim of conservatism and fast computation through experiments.

## I. INTRODUCTION

Future planetary missions will require long-distance autonomous traverse on challenging, obstacle-rich terrains. For example, one of the top candidate sites for the NASA/JPL Mars 2020 (M2020) mission is the Jezero crater, a 49 [km]-wide crater considered to be an ancient Martian lake produced by the past water-related activities [1]. Despite its scientific richness, significant engineering challenges are to be expected because of the rock abundance inside the crater. The current surface mobility software [2] is designed to operate in modestly-cluttered terrain of about 7% rock abundance in Cumulative Fractional Area (CFA) measure [3], and its performance is known to be drastically degraded over 10% CFA. The Mars Science Laboratory (MSL) Curiosity rover (Fig. 1) was deployed in the Gale crater where the surface is mostly covered with 10% rock CFA. Even in

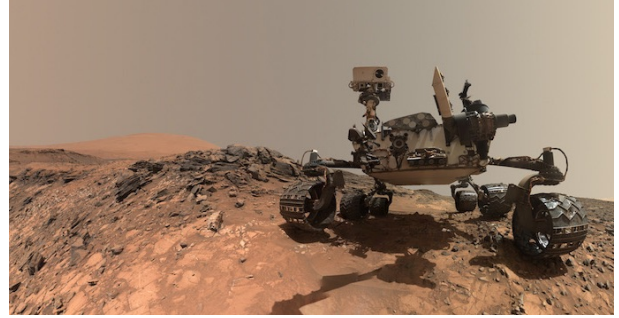


Fig. 1: Self-portrait of the MSL Curiosity rover, taken on Sol 1065. Sufficient clearance between the vehicle and the ground is necessary to safely traverse on rough terrain with outcrops. (Credit: NASA/JPL-Caltech/MSSS)

this modest terrain, the use of the autonomous navigation (AutoNav) driving mode is restricted to benign terrain to ensure safety. The rock abundance in the Jezero crater is higher than Gale, ranging up to 15–20% in the satellite-based map [4]. Such dense hazard distributions pose crucial challenges for traversability, and motivated the development of a new motion-planning algorithm for the M2020 rover.

To navigate rovers in a cluttered environment, a path planner should be aware of the wheel placement, and ensure that the configuration does not violate any safety metrics, such as attitude, suspension limits, and clearance between the rover belly pan and the ground. Evaluating these metrics requires solving an iterative inverse-kinematics problem, which is not tractable given the very limited computational resources of the planetary rovers. Besides the nonlinear kinematics equations associated with the suspension mechanisms, a rough terrain profile makes it difficult to precisely predict wheel-terrain contact. There are no known analytic solutions in general, and the problem is typically approached by iterative numerical methods at the cost of computational efficiency.

A numeric kinematics solution using the iterative Newton-Raphson method has been used in the ground operations (as opposed to on-board path planning) of Mars rovers [5], [6]. An alternative simplified kinematics approach is employed in [7], which iteratively minimizes the residual between the wheel and terrain elevations given static rover position and heading on the height map. In [8], [9], a full kinematic and dynamic simulation is conducted based on the Rover Analysis Modeling and Simulation (ROAMS) framework [10], [11]. ROAMS also uses the Newton-Raphson method to solve the kinematic state of the rover, and also includes a multi-body dynamics simulation to accurately model the rover behavior on rough terrain. A similar approach is per-

\*This research was carried out at the Jet Propulsion Laboratory, California Institute of Technology, under a contract with the National Aeronautics and Space Administration. Copyright 2018 California Institute of Technology. U.S. Government sponsorship acknowledged.

<sup>1</sup>Kyohei Otsu, Masahiro Ono, and Olivier Toupet are with Jet Propulsion Laboratory, California Institute of Technology, Pasadena, CA, U.S.A., {otsu, ono, otoupet}@jpl.nasa.gov

<sup>2</sup>Guillaume Matheron is with École Normale Supérieure de Paris, France, guillaume.pub@matheron.eu

<sup>3</sup>Sourish Ghosh is with Indian Institute of Technology, Kharagpur, India, sourishg@iitkgp.ac.in

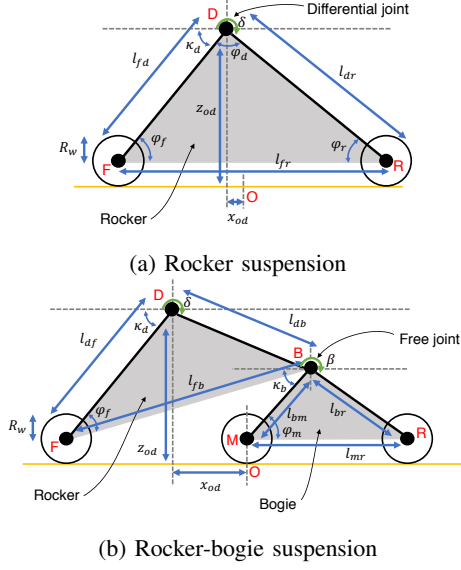


Fig. 2: Articulated suspension systems on flat ground, viewed from the left side.

formed for articulated tracked vehicles [12]. Although these methods can fairly accurately estimate clearance, vehicle attitude, and suspension angles, they cannot directly be deployed onto the rovers due to its intractable computational cost. Moreover, for on-board path planning in planetary missions, conservatism is more important than accuracy: a single collision can terminate a mission as it is not possible to repair a damaged vehicle on another planet at least for the foreseeable future.

The main contribution of this paper is to introduce a novel inverse-kinematics solution named Approximate Clearance Evaluation (ACE). The key concept of ACE is to quickly compute the vehicle configuration bounds, instead of solving the full kinematic rover-terrain settling. Knowing the bounds of certain key states, ACE can effectively produce a conservative estimation of the rover-terrain clearance, rover attitude, and suspension angles. ACE is being developed as part of the autonomous surface navigation software of NASA/JPL's M2020 mission. The initial idea of ACE appears in [13]. This paper introduces improved mathematical formulation and extensive Verification and Validation (V&V) work.

The remainder of this paper is structured as follows: Section II formulates the kinematics models of articulated suspension systems, Section III describes the ACE algorithm, Section IV provides experimental results including benchmarking, and Section V concludes the paper.

## II. SUSPENSION MODELS

Our approach is to use kinematic equations to propagate the bounds on the height of wheels to the bounds on vehicle configuration. While this approach is applicable to vehicles with articulated suspension systems in general, the kinematics model described in this section focuses on the rocker and rocker-bogie suspensions (Fig. 2 and 3). The latter is the suspension system of choice for the successful NASA/JPL's Mars rover missions.

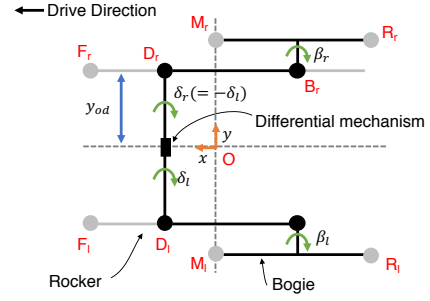


Fig. 3: Rocker-bogie suspension model, viewed from top. For visibility, wheels do not represent actual positions.

### A. Frames

We first introduce the reference frames used in the paper. Following the aerospace convention, the forward-right-down coordinate system is employed for the body frame of the rover. The origin is set to the center of middle wheels at the height of ground contact point when the rover is stationary on the flat ground. In this frame, the wheel heights are described in  $z$ -axis pointing downward. (A greater wheel “height” indicates that the wheel is shifted downward.)

A global reference frame is defined as a north-east-down coordinate system. The terrain geometry, which can be specified in any format such as a point cloud or a Digital Elevation Map (DEM), is expressed in this frame. In this paper, we assume that motion planning is performed in the global frame. Considering the nature of rover mobility, we assume that the planning is done in 2D or 2.5D space. A path is represented as a set of  $(x, y, \psi)$  states. If all poses along a path satisfies the safety constraints, the path is regarded as collision-free.

### B. Rocker Suspension

The rocker suspension in Fig. 2(a) is a simpler variant of the rocker-bogie suspension, which will be discussed in the next section. The rocker suspension usually consists of four wheels, where the two wheels on the same side are connected with a rigid rocker link. The left and right suspensions are related through a passive differential mechanism, which transfers a positive angle change on one side as a negative change to the other side.

The kinematic relation of the rocker suspension is represented by a simple triangular geometry in Fig. 4. Consider a triangle ABC with a known shape parameterized by two side lengths and the angle between them  $(l_{ca}, l_{ab}, \varphi_a)$ . Given the height of A and B (i.e.,  $z_a, z_b$ ), there are up to four solutions for  $z_c$ , but other constraints such as vehicle orientation uniquely specifies a single solution given by:

$$z_c = z_a - l_{ca} \sin \kappa(z_a, z_b) \quad (1)$$

where  $\kappa(\cdot)$  denotes an angle of link AC with respect to the reference line and is defined as

$$\kappa(z_a, z_b) = \varphi_a + \sin^{-1} \left( \frac{z_a - z_b}{l_{ab}} \right). \quad (2)$$

The solution only exists if  $|z_a - z_b| \leq l_{ab}$ .

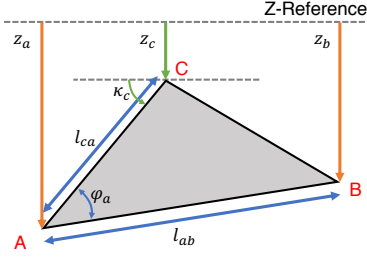


Fig. 4: Triangular geometry.

The rocker suspension model is formulated using the triangular geometry in (1) and (2). Given two wheel heights  $z_f$  and  $z_r$ , the rocker joint height is given as

$$z_d = z_f - l_{df} \sin \kappa_d(z_f, z_r) \quad (3)$$

where  $l_{df}$  is the length of front rocker link and  $\kappa_d(\cdot)$  is an instance of (2) with the rocker suspension parameters ( $l_{df}, l_{fr}, \phi_f$ ). Due to the differential mechanism, the left and right rocker angles in relative to the body,  $\delta_l, \delta_r$ , have the same absolute value with the opposite sign. They can be computed from link angles as:

$$\delta_l = -\delta_r = \frac{\kappa_d(z_{fr}, z_{rr}) - \kappa_d(z_{fl}, z_{rl})}{2} \quad (4)$$

The body attitude is a function of left and right rocker joint states. The roll angle of the body is computed from the difference of joint heights:

$$\phi = \sin^{-1} \left( \frac{z_{dr} - z_{dl}}{2y_{od}} \right), \quad (5)$$

where  $y_{od}$  is the lateral offset from the center of body to a differential joint. The pitch angle is computed as

$$\theta = \kappa_{d0} - \frac{\kappa_d(z_{fl}, z_{rl}) + \kappa_d(z_{fr}, z_{rr})}{2} \quad (6)$$

where the first term represents an angle offset of front link when the rover is on a flat ground ( $\kappa_{d0} = \phi_f$  in this example).

Finally, the body frame height in the global frame can be obtained as

$$z_o = \frac{z_{dl} + z_{dr}}{2} + x_{od} \sin \theta \cos \phi - z_{od} \cos \theta \cos \phi \quad (7)$$

where  $x_{od}$  and  $z_{od}$  are offsets from the body frame origin to a differential joint. Since the belly pan is rigidly attached to the body frame, the rover-terrain clearance can be derived from these height and attitude information.

### C. Rocker-bogie Suspension

The rocker-bogie suspension (Fig. 2(b)) is a rocker suspension with an additional free joint on each side. According to the previous Mars rover conventions, we assume that the front wheels of the six-wheeled rover are connected directly to the rocker suspension while the middle and rear wheels are attached to the bogie suspension. The inverse kinematics of the rocker-bogie suspension can be derived by extending that of the rocker suspension, described in the previous subsection.

We first determine the state of bogie link. The bogie joint heights can be estimated from middle and rear wheel heights ( $z_m, z_r$ )

$$z_b = z_m - l_{bm} \sin \kappa_b(z_m, z_r) \quad (8)$$

where  $l_{bm}$  is the length of bogie front link and  $\kappa_b(\cdot)$  denotes the triangular geometry for the bogie triangle. Using the height of bogie joint  $z_b$ , the rocker joint height can be computed as

$$z_d = z_f - l_{df} \sin \kappa_d(z_f, z_b). \quad (9)$$

Given the heights of the wheels and joints, rocker and bogie angle changes are computed as

$$\delta_l = -\delta_r = \frac{\kappa_d(z_{fr}, z_{br}) - \kappa_d(z_{fl}, z_{bl})}{2} \quad (10)$$

$$\beta_l = \kappa_d(z_{fl}, z_{bl}) - \kappa_b(z_{ml}, z_{rl}) - \kappa_{d0} + \kappa_{b0} \quad (11)$$

$$\beta_r = \kappa_d(z_{fr}, z_{br}) - \kappa_b(z_{mr}, z_{rr}) - \kappa_{d0} + \kappa_{b0} \quad (12)$$

where  $\kappa_{d0}$  and  $\kappa_{b0}$  denote the initial angles of rocker and bogie joints. The attitude and height of the body are derived as:

$$\phi = \sin^{-1} \left( \frac{z_{dr} - z_{dl}}{2y_{od}} \right) \quad (13)$$

$$\theta = \kappa_{d0} - \frac{\kappa_d(z_{fl}, z_{bl}) + \kappa_d(z_{fr}, z_{br})}{2} \quad (14)$$

$$z_o = \frac{z_{dl} + z_{dr}}{2} + x_{od} \sin \theta \cos \phi - z_{od} \cos \theta \cos \phi. \quad (15)$$

### III. ALGORITHM

Remind that ACE is designed to quickly compute conservative bounds on vehicle states. Unlike the full kinematics settling that depends on iterative numerical methods, our approach computes the bounds in a closed form. The ACE algorithm is summarized as follows:

- 1) For a given target rover pose  $(x, y, \psi)$ , find a rectangular wheelbox in x-y plane that conservatively includes the footprint of each wheel over any possible rover attitude and suspension angles.
- 2) Find the minimum and maximum terrain heights in each of the wheelboxes (see Fig. 5).
- 3) Propagate the bounds on wheel heights to the vehicle configuration with the kinematic formula derived in the previous section.
- 4) Assess vehicle safety based on the worst-case states.

In 3), all possible combinations are considered to obtain the worst-case bounds. Due to the monotonic nature of suspension, the bounds can be obtained via the evaluation of extreme configurations. For example, the bounds on the rocker/bogie states are obtained by finding the worst cases among the eight extreme combinations of the min/max heights of three wheels, as illustrated in Fig. 6. This propagation process is visually presented in the supplemental video.

To precisely describe the algorithm, we first introduce the interval arithmetic as a mathematical framework in our method. We then describe how we apply it to solve our problem with a case study using the Curiosity rover.

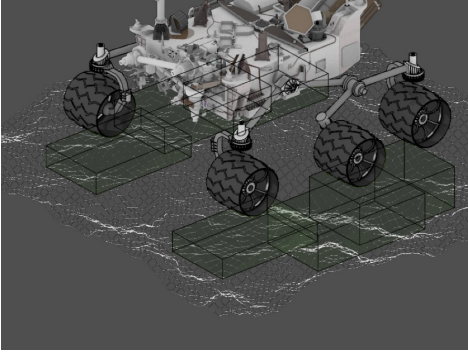


Fig. 5: Ranges of possible wheel configurations computed from terrain geometry and mechanical constraints.

#### A. Notation

In the interval arithmetic [14], an *interval* is defined as follows

$$[x^-, x^+] = \{x \in \mathbb{R}^* \mid x^- \leq x \leq x^+\} \quad (16)$$

where a pair  $[x^-, x^+]$  represents the all reals between two. The symbol  $\mathbb{R}^*$  denotes an extended real defined as  $\mathbb{R}^* = \mathbb{R} \cup \{-\infty, \infty\}$ . Elementary arithmetic operations on reals can be extended to intervals, such as

$$[x^-, x^+] + [y^-, y^+] = [x^- + y^-, x^+ + y^+] \quad (17)$$

$$[x^-, x^+] - [y^-, y^+] = [x^- - y^+, x^+ - y^-] \quad (18)$$

For a continuous function  $f(x)$ , we can extend its input and output space to intervals

$$f([x^-, x^+]) = \left[ \min_{x \in [x^-, x^+]} f(x), \max_{x \in [x^-, x^+]} f(x) \right]. \quad (19)$$

Computing the minimum and maximum is trivial if the function  $f$  is monotonic, or special non-monotonic functions such as trigonometric functions.

In the rest of the paper, we use the following abbreviation to represent an interval unless explicitly stated

$$[x] \equiv [x^-, x^+]. \quad (20)$$

#### B. Wheel Height Intervals

Firstly, we estimate the wheel height intervals from terrain measurements. Because of mechanical constraints (endpoints and vehicle stability), we have bounds on the suspension angles and the roll of the rover. Given these bounds, we can compute bounds on the  $x$  and  $y$  position of each wheel's center. Knowing the size of the wheels, and assuming the contact point between a wheel and the ground is on the lower half of the wheel, we compute  $x$  and  $y$  bounds on the terrain points that may be in contact with each wheel (see Fig. 5).

From the terrain data reconstructed from sensors such as stereo vision, we can compute the bounds on the height for each wheel. We represent the bound for  $i$ -th wheel by  $[z_i]$ . It is important to estimate these bounds conservatively to make the final state bounds to be complete, since the uncertainty in wheel heights is directly propagated to other states. For the conservative estimate, we may need to include the dynamic

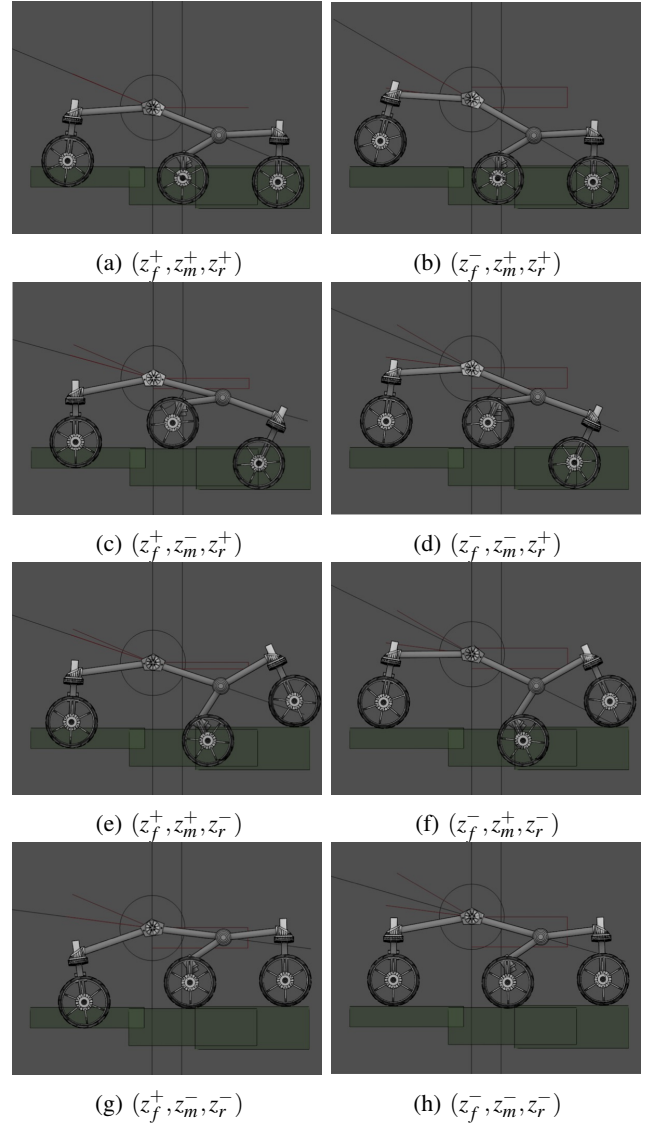


Fig. 6: Extreme configurations for state bound computation. Three elements in a tuple represent the front, middle and rear wheel heights, respectively. The superscripts  $+$  and  $-$  represent the maximum and minimum for the state variable.

effect such as terrain deformation, wheel slips and sinkage, depending on the environment to explore.

#### C. Suspension Intervals

Since  $\sin^{-1}(x)$  is monotonically increasing in  $x \in [-1, 1]$ , we can extend the concept of intervals to the function  $\kappa(\cdot)$  in (2)

$$\kappa([z_a], [z_b]) = [\kappa(z_a^-, z_b^+), \kappa(z_a^+, z_b^-)] \quad (21)$$

On the other hand, (1) is a convex function which has a global minimum if  $z_b = z_b^-$  and the rear link CB is aligned with  $z$ -axis. In case of the Curiosity rover, the minimum is located outside of the mechanical limits. Therefore, in practice, we can assume the monotonicity and use the following interval for the height

$$[z_c] = [z_a^- - l_{ab} \sin \kappa_b(z_a^-, z_b^-), z_a^+ - l_{ab} \sin \kappa_b(z_a^+, z_b^+)]. \quad (22)$$



Based on the above intervals, the suspension state intervals are computed for joint heights

$$[z_b] = [z_m^- - l_{bm} \sin \kappa_b(z_m^-, z_r^-), z_m^+ - l_{bm} \sin \kappa_b(z_m^+, z_r^+)] \quad (23)$$

$$[z_d] = [z_f^- - l_{df} \sin \kappa_d(z_f^-, z_b^-), z_f^+ - l_{df} \sin \kappa_d(z_f^+, z_b^+)] \quad (24)$$

and for joint angles

$$[\delta_l] = -[\delta_r] \quad (25)$$

$$= \left[ \frac{\kappa(z_{f_l}^-, z_{b_l}^+) - \kappa_d(z_{f_l}^+, z_{b_l}^-)}{2}, \frac{\kappa(z_{f_r}^+, z_{b_r}^-) - \kappa_d(z_{f_r}^-, z_{b_r}^+)}{2} \right] \quad (26)$$

$$[\beta_l] \subseteq \left[ \kappa_d(z_{f_l}^-, z_{b_l}^+) - \kappa_b(z_{m_l}^+, z_{r_l}^-) - \kappa_{d0} + \kappa_{b0}, \right. \\ \left. \kappa_d(z_{f_l}^+, z_{b_l}^-) - \kappa_b(z_{m_l}^-, z_{r_l}^+) - \kappa_{d0} + \kappa_{b0} \right] \quad (27)$$

$$[\beta_r] \subseteq \left[ \kappa_d(z_{f_r}^-, z_{b_r}^+) - \kappa_b(z_{m_r}^+, z_{r_r}^-) - \kappa_{d0} + \kappa_{b0}, \right. \\ \left. \kappa_d(z_{f_r}^+, z_{b_r}^-) - \kappa_b(z_{m_r}^-, z_{r_r}^+) - \kappa_{d0} + \kappa_{b0} \right] \quad (28)$$

Note that the intervals for the bogie angles are obtained as loose bounds.

#### D. Attitude intervals

Similarly, the intervals for body attitude can be derived from wheel height intervals. Using the kinematics equations (13) and (14) yields

$$[\phi] = \left[ \sin^{-1} \left( \frac{z_{d_r}^- - z_{d_l}^+}{2y_{od}} \right), \sin^{-1} \left( \frac{z_{d_r}^+ - z_{d_l}^-}{2y_{od}} \right) \right] \quad (29)$$

$$[\theta] = \left[ \kappa_{d0} - \frac{\kappa_d(z_{f_l}^+, z_{b_l}^-) + \kappa_d(z_{f_r}^+, z_{b_r}^-)}{2}, \right. \\ \left. \kappa_{d0} - \frac{\kappa_d(z_{f_l}^-, z_{b_l}^+) + \kappa_d(z_{f_r}^-, z_{b_r}^+)}{2} \right] \quad (30)$$

#### E. Clearance Intervals

Since the vehicle body has connection to the world only through its suspension and wheel systems, its configuration is fully determined by the suspension state. The body height bound in the world frame is computed with (15):

$$[z_o] \subseteq \left[ \frac{z_{d_l}^- + z_{d_r}^-}{2} - z_{od} \cos |\theta|^+ \cos |\phi|^+ \right. \\ \left. + x_{od} \min(\sin \theta^- \cos |\phi|^-, \sin \theta^- \cos |\phi|^+), \right. \\ \left. \frac{z_{d_l}^+ + z_{d_r}^+}{2} - z_{od} \cos |\theta|^- \cos |\phi|^- \right. \\ \left. + x_{od} \max(\sin \theta^+ \cos |\phi|^-, \sin \theta^+ \cos |\phi|^+) \right]. \quad (31)$$

using the intervals of absolute roll/pitch angles  $[|\phi|], [|\theta|]$ . Note that the trigonometric functions in the equations are monotonic since we can assume  $|\phi|, |\theta| \in [0, \frac{\pi}{2}]$  for typical rovers. Assuming the belly pan is represented as a plane with width  $w_p$  and length  $l_p$  at nominal ground clearance

$c_0$ , a loose bound for the maximum (lowest) height point in belly pan is computed as

$$[z_p] \subseteq [z_o^- - c_0 \cos |\theta|^- \cos |\phi|^- \\ + \frac{l_p}{2} \sin |\theta|^- \cos |\phi|^+ + \frac{w_p}{2} \sin |\phi|^-, \\ z_o^+ - c_0 \cos |\theta|^+ \cos |\phi|^+ \\ + \frac{l_p}{2} \sin |\theta|^+ \cos |\phi|^- + \frac{w_p}{2} \sin |\phi|^+] \quad (32)$$

Let's define the rover-ground clearance as a height gap between the lowest point of the belly pan and the highest point of the ground. This is a conservative estimate of clearance. Given the intervals of ground point height under the belly pan  $[z_m]$ , the clearance is computed as

$$[c] \equiv [z_m^- - z_p^+, z_m^+ - z_p^-]. \quad (33)$$

#### F. Safety Metrics

We use the above state intervals to test if a given pose has chance to violate safety conditions. Different safety conditions can be applied to different rovers. For example, the following metrics are considered for the M2020 rover.

- *Ground clearance* must be greater than a threshold.
- *Body tilt* (computed from roll and pitch angles) must be smaller than a threshold.
- *Suspension angles* must stay within predefined safety ranges.
- *Wheel drop* (defined as a span of wheel height uncertainty) must be smaller than a threshold.

### IV. EXPERIMENTS

In this section, we present the simulation results to validate our approach. The algorithm is tested on two terrain configurations: simple flat terrain with a bump and synthetic Martian terrains with simulated rock distribution. We used numerical methods to obtain ground-truth rover settling. The results illustrate the validity of the computed intervals to represent the bounds of the state variables.

#### A. Flat Terrain with a Bump

The first test environment is a simple flat terrain with a 0.2 [m] height bump. The Curiosity-sized rover is driven over the bump with three different trajectories. These trajectories are evaluated using our method and a baseline numerical method [5]. Fig. 7 shows the time-series profiles of suspension and body states for three trajectories shown in Fig. 8. The solid lines denote the ground-truth states computed by the numeric method, and the shaded regions represent the state bounds computed by ACE. As can be seen, all states are properly bounded by the ACE intervals.

ACE computes the state bounds based on the evaluation of worst-case configurations. This effect is noticeable for linear trajectory (a). In the top left figure of Fig. 7, the ground-truth roll angle stays zero for the entire trajectory, while there are a few degrees of perturbation in ACE bounds. This perturbation is a result of capturing potential time lag between the left and right wheels' contact time to the bump.

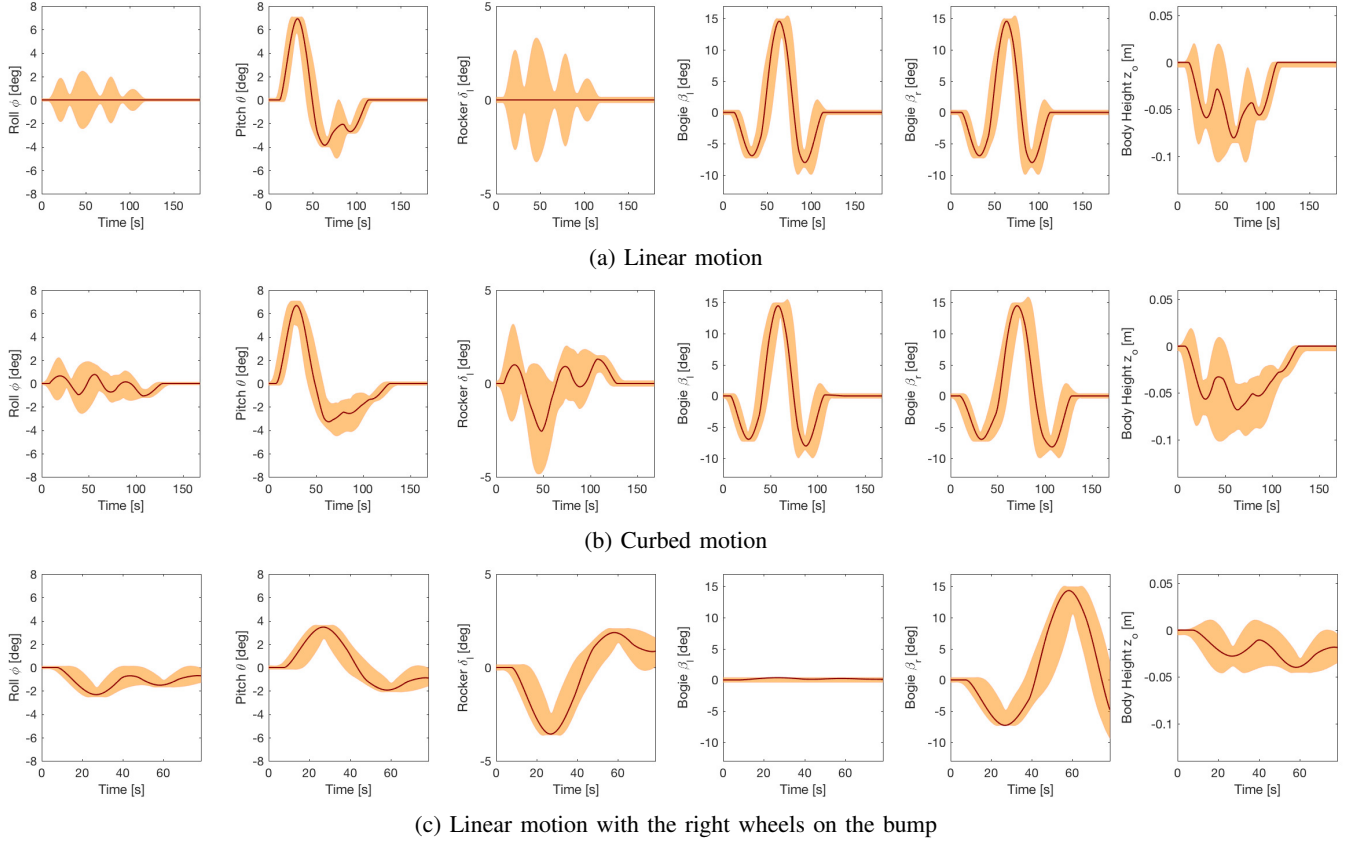


Fig. 7: ACE estimation results for body roll  $\phi$ , body pitch  $\theta$ , left rocker angle  $\delta_l$ , left and right bogie angles  $\beta_l$  and  $\beta_r$ , and body height  $z_o$ . The solid lines represent the ground-truth state computed by a numeric method. The shaded regions represent the ranges between the ACE upper/lower bounds.

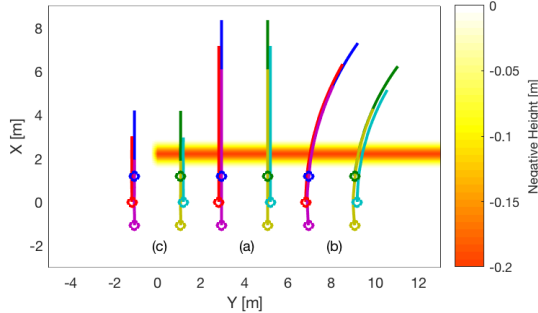


Fig. 8: Flat terrain with a smooth bump. a) Linear approach to the bump. b) Curved approach to the bump. c) Climb over the bump only with the right wheels.

If there is a lag between two wheel contact, we will observe a rolling effect of the vehicle as we see it for curved motion (b). The results are consistent with our claim that ACE always provides conservative bounds.

### B. Martian Terrain Simulation

Next, we tested the ACE algorithm with the ROAMS simulator [10]. We imported a Martian terrain model generated from satellite imagery, and randomly synthesized rocks based on the empirical size distribution model proposed by [3]. For

the rover platform, we used the Rocky 8 rover which is a mid-sized rover similar to Mars Exploration Rovers (MERs). The simulation environment is shown in Fig. 9.

The state estimation result is shown in Fig. 10. Only the body states including roll, pitch, and minimum clearance are reported, but similar results are obtained for the other suspension states. It is clearly seen that the ground-truth values reside inside the ACE upper/lower bounds. The spans for state bounds are larger in this result, mainly because i) noisy terrain data increase the wheel height uncertainty, and ii) the smaller vehicle size amplifies the effect of terrain roughness. Fig. 11 shows the statistical results for the safety metrics. As for the max tilt, the worst-case estimate is always larger than the ground-truth. Same for minimum clearance, except that the estimate is always smaller than the ground-truth. These results indicate that ACE always provides conservative safety assessment.

### C. Run-time Performance

Unlike numerical methods, the computation time of ACE is independent of terrain complexity. The average run-time over 1000 independent trials is about 2 [ $\mu$ s] with very little deviation, measured on a 2.8 GHz Intel Core i7 machine using only a single core. We also ran ACE on the RAD750 CPU, which is used for the Curiosity and Mars 2020 rovers.

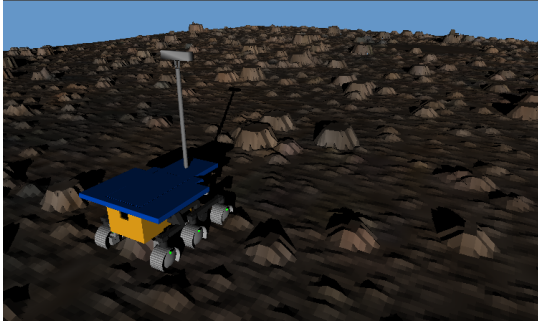


Fig. 9: The Rocky 8 rover on synthetic Martian terrain. The base terrain is an orbit-based DEM for the Jezero crater. The rocks are randomly populated according to the Martian size-frequency distribution of rocks.

While the precise timing is difficult due to the specialized configuration of the flight software, the typical runtime was 10-15 [ms] with a 10 [cm] resolution DEM.

## V. CONCLUSIONS

In this paper, an approximate kinematics solver was presented that can quickly, albeit conservatively, evaluate the state bounds of articulated suspension systems, thus providing a tractable way of determining path safety with the limited computational resources available to planetary rovers. ACE avoids expensive iterative operations by only solving for the worst-case rover-terrain configurations. The algorithm is validated using simulations, where it was shown that the computed intervals do always contain the ground-truth states. The ACE algorithm is successfully integrated with the M2020 surface navigation software, and will enable faster autonomous traverse in more challenging terrains on the red planet.

## REFERENCES

- [1] T. A. Goudge, J. F. Mustard, J. W. Head, C. I. Fassett, and S. M. Wiseman, "Assessing the mineralogy of the watershed and fan deposits of the Jezero crater paleolake system, Mars," *Journal of Geophysical Research: Planets*, vol. 120, no. 4, pp. 775–808, 2015.
- [2] M. Maimone, J. Biesiadecki, E. Tunstel, Y. Cheng, and C. Leger, "Surface navigation and mobility intelligence on the Mars Exploration Rovers," in *Intelligence for Space Robotics* (A. Howard and E. Tunstel, eds.), ch. 3, pp. 45–69, 2006.
- [3] M. Golombek and D. Rapp, "Size-frequency distributions of rocks on Mars and Earth analog sites: implications for future landed missions," *Journal of Geophysical Research: Planets*, vol. 102, no. E2, pp. 4117–4129, 1997.
- [4] M. Golombek, J. W. Ashley, A. Huertas, R. Fergason, and R. Kirk, "Terrain characterization: approach and results," in *Mars 2020 Landing Site Workshop*, 2015.
- [5] J. Yen, B. Cooper, F. Hartman, S. Maxwell, and J. Wright, "Sequence Rehearsal and Validation for Surface Operations of the Mars Exploration Rovers," in *AIAA Space Ops Conference*, pp. 1–7, 2004.
- [6] J. Wright, F. Hartman, B. Cooper, S. Maxwell, J. Yen, and J. Morrison, "Driving on the surface of mars with the Rover Sequencing and Visualization Program," in *IEEE Society of Instrumentation and Control Engineers*, 2005.
- [7] T. Howard and A. Kelly, "Optimal rough terrain trajectory generation for wheeled mobile robots," *The International Journal of Robotics Research*, vol. 26, pp. 141–166, 2007.

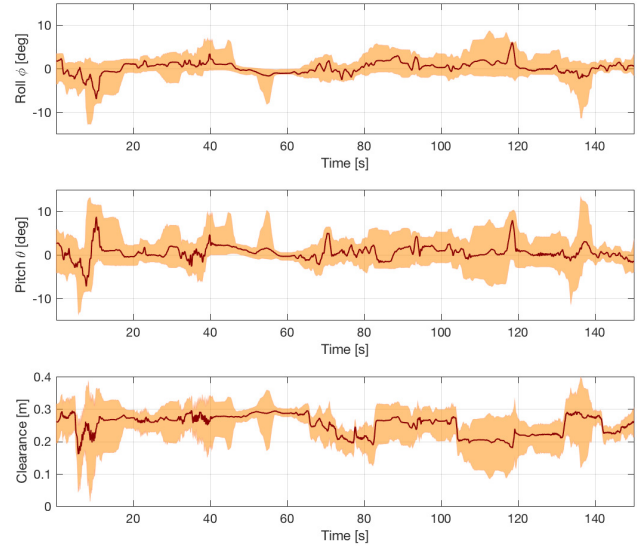


Fig. 10: ACE estimation result for Martian environment. Time-series ground-truth data are presented for roll/pitch angles and ground clearance with ACE upper/lower bounds.

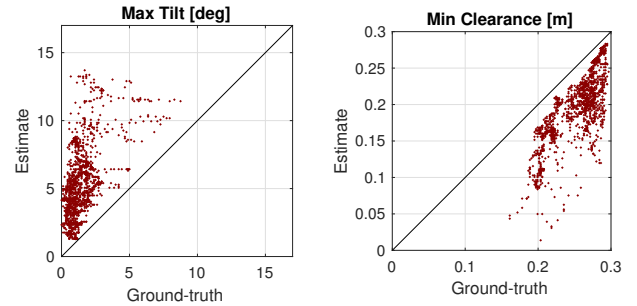


Fig. 11: Safety metric statistics from Martian terrain simulation. The algorithm always produces the conservative estimate.

- [8] T. Huntsberger, A. Jain, J. Cameron, G. Woodward, D. Myers, and G. Sohl, "Characterization of the ROAMS simulation environment for testing rover mobility on sloped terrain," in *International Symposium on Artificial Intelligence, Robotics, and Automation in Space*, 2008.
- [9] D. Helmick, A. Angelova, and L. Matthies, "Terrain adaptive navigation for planetary rovers," *Journal of Field Robotics*, vol. 26, no. 4, pp. 391–410, 2009.
- [10] A. Jain, J. Guineau, C. Lim, W. Lincoln, M. Pomerantz, G. Sohl, and R. Steele, "ROAMS: planetary surface rover simulation environment," in *International Symposium on Artificial Intelligence, Robotics and Automation in Space*, pp. 19–23, 2003.
- [11] A. Jain, J. Balaram, J. Cameron, J. Guineau, C. Lim, M. Pomerantz, and G. Sohl, "Recent developments in the ROAMS planetary rover simulation Environment," in *IEEE Aerospace Conference*, vol. 2, pp. 861–876, 2004.
- [12] P. Papadakis and F. Pirri, "3D mobility learning and regression of articulated, tracked robotic vehicles by physics-based optimization," in *Workshop on Virtual Reality Interaction and Physical Simulation, Eurographics*, pp. 147–156, 2012.
- [13] K. Otsu, *Study on Robotic Intelligence for Vision-based Planetary Surface Navigation*. PhD thesis, The University of Tokyo, 2016.
- [14] T. Hickey, Q. Ju, and M. H. van Emden, "Interval arithmetic: From principles to implementation," *Journal of the ACM*, vol. 48, no. 5, pp. 1038–1068, 2001.